Structural Studies on 24P-IκBα Peptide Derived from a Human IκB-α Protein Related to the Inhibition of the Activity of the Transcription Factor NF-κB †

ARTICLE *in* BIOCHEMISTRY · APRIL 2007

Impact Factor: 3.02 · DOI: 10.1021/bi061401f · Source: PubMed

7 AUTHORS, INCLUDING:

Julien Pons
Rectorat de Corse
9 PUBLICATIONS **143** CITATIONS
SEE PROFILE

Nathalie Evrard-Todeschi
Université René Descartes - Paris 5
25 PUBLICATIONS **358** CITATIONS
SEE PROFILE

Gildas Bertho
Université René Descartes - Paris 5
70 PUBLICATIONS **971** CITATIONS
SEE PROFILE

Structural Studies on 24P-IκBα Peptide Derived from a Human IκB-α Protein Related to the Inhibition of the Activity of the Transcription Factor NF-κB†

Julien Pons,‡ Nathalie Evrard-Todeschi,‡ Gildas Bertho,‡ Josyane Gharbi-Benarous,‡ Vanessa Sonois,‡ Richard Benarous,§ and Jean-Pierre Girault*,‡

Université Paris V-René Descartes, Laboratoire de Chimie et Biochimie Pharmacologiques et Toxicologiques (UMR 8601 CNRS), 45 rue des Saint-Pères, 75270 Paris Cedex 06, France, and Université Paris V-René Descartes, U567-INSERM, UMR 8104 CNRS, Institut Cochin-Département des Maladies Infectieuses, Hôpital Cochin Bat. G. Roussy, 27 rue du Faubourg St-Jacques, 75014 Paris, France

Received July 12, 2006; Revised Manuscript Received November 13, 2006

ABSTRACT: The IκB-α protein, inhibitor of the transcription factor nuclear factor-κB (NF-κB), is a cellular substrate of β-transducin repeat containing protein (β-TrCP). β-TrCP is the F-box protein component of an Skp1/Cul1/F-box (SCF)-type ubiquitin ligase complex. β-TrCP targets the protein IκB-α for ubiquitination, followed by proteasome degradation. The SCF−β-TrCP complex specifically recognizes an IκB-α peptide containing the D**pS**GXX**pS** motif in a phosphorylation-dependent manner. A fragment comprising 24 amino acids residues for the phosphorylated peptide at the two sites Ser32 and Ser36 and thus termed 24P-IκBα (P-IκBα$^{21-44}$) was characterized conformationally by NMR spectroscopy and molecular dynamics simulation. In the free states, 24P-IκBα exhibits mainly a random coil conformation, although the presence of a nascent bend was detected between residues 30 and 36, flanked by two N- and C-terminal disordered regions. The bound conformation of the phosphorylated IκB-α peptide was obtained using transfer nuclear Overhauser effect spectroscopy (TRNOESY) experiments. To further elucidate the basis of the β-TrCP interaction, a complex between 24P-IκBα peptide and β-TrCP protein was studied using saturation transfer difference (STD) NMR experiments. The conformation of 24P-IκBα bound to β-TrCP presents a bend corresponding to the ^{31}D**pS**GLD**pS**^{36} motif and on both sides N- and C-terminal turn regions (Lys22−Asp31 and Met37−Glu43). The bound structure of the phosphorylated peptide suggests that these domains are crucial for the interaction of the peptide with its receptor showing the protons identified by STD NMR as exposed in close proximity to the β-TrCP surface.

NF-κB[1] is a transcriptional activator that under resting conditions resides in the cytoplasm in an inactive complex with its inhibitor IκB-α (*1*, *2*). Degradation of IκB-α following stimulation of cells by growth factors, chemokines, or inflammatory cytokines such as TNF-α leads to activation of NF-κB and its translocation into the nucleus, where it induces target gene expression. The excessive degradation of IκB-α is implied in chronic inflammatory pathologies. NF-κB plays a central role in the expression of numerous genes encoding cytokines, chemokines, and factors involved in T-cell activation and proliferation (*1*, *2*). In addition, NF-κB has been implicated in the control of antiapoptotic genes (*3*, *4*). Thus, NF-κB is a pivotal transcription factor that controls inflammation pathways and other stressful situations. Activation of NF-κB, under the control of IκB degradation, is the hallmark of the innate immune response (*5*). High constitutive activation of NF-κB is implicated in all chronic inflammatory syndromes. NF-κB is also a key player in the aetiology of solid tumors and can promote tumor cell survival and reduce the effectiveness of anticancer therapy. Hence, targeting NF-κB activation pathways would allow development of new anti-inflammatory and anticancer drugs.

The SCF−β-TrCP was shown to mediate the ubiquitination and proteasome targeting of the NF-κB-inhibitory molecule IκB-α (*6*, *7*) (Figure 1). The ubiquitin−proteasome pathway of protein degradation is essential for various important biological processes including cell-cycle progression, gene transcription, and signal transduction (*8*−*10*). Human β-TrCP is a key component of a recently characterized E3 ubiquitin ligase complex that regulates protein

† This work was supported by grants from Sidaction and ANRS.

* To whom correspondence should be addressed. Phone: (33) 1 42 86 21 80. Fax: (33) 1 42 86 83 87. E-mail: jean-pierre.girault@univ-paris5.fr.

§ Institut Cochin-Département des Maladies Infectieuses.

‡ Laboratoire de Chimie et Biochimie Pharmacologiques et Toxicologiques.

[1] Abbreviations: β-TrCP, transducin repeat containing protein; FID, free induction decay; GST, glutathione S transferase; HIV, human immunodeficiency virus; HMBC, heteronuclear multiple-bond correlation; HSQC, heteronuclear single quantum correlation; INEPT, insensitive nuclei enhanced by polarization transfer; MD, molecular dynamics; NOESY, nuclear Overhauser effect spectroscopy; NF-κB, nuclear factor-κB; PBS, phosphate-buffered saline; rmsd, root mean square deviation; SCF, Skp1−Cullin−F-Box; STD, saturation transfer difference; TFE, 2,2,2-trifluoroethanol; TRNOESY, transferred nuclear Overhauser effect spectroscopy; TOCSY, total correlation spectroscopy; TPPI, time-proportional phase incrementation; Vpu, HIV-1 encoded virus protein U; Watergate, water suppression by gradient-tailored excitation; WD domain, Trp−Asp domain; pS, phosphorylated serine.

10.1021/bi061401f CCC: $37.00
Published on Web 02/24/2007

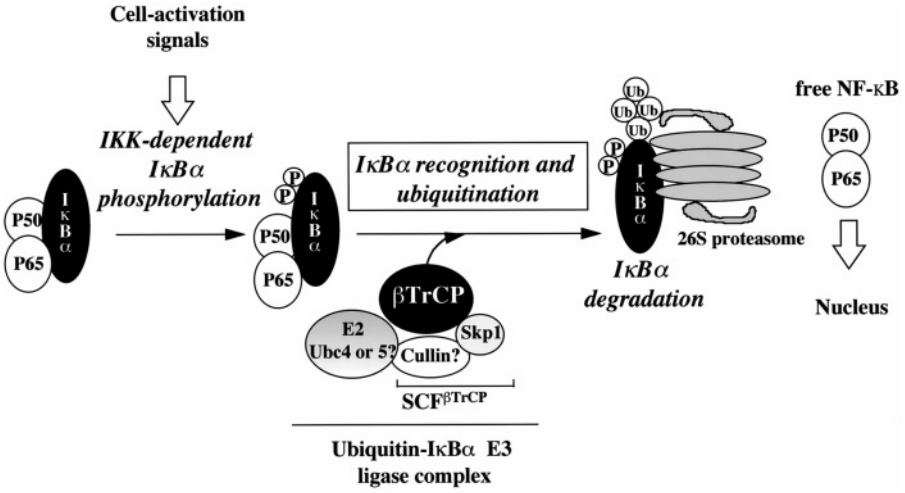

FIGURE 1: A model for the role of β-TrCP in the proteolysis of IκB-α and NF-κB activation. Upon cell activation and IκB-α phosphorylation, β-TrCP interacts with Ser32−Ser36 phosphorylated IκB-α but not with unmodified IκB-α. In the SCF−β-TrCP complex, β-TrCP allows recognition of IκB-α and triggers the E3-dependent ubiquitination that ultimately marks IκB-α for the proteolytic attack by the 26S proteasome. Degradation of IκB-α releases the transcription factor NF-κB, which localizes to the nucleus (*61*).

Table 1. Sequence of Three Peptide Ligands of the β-TrCP Protein

name	sequence number	sequence
24P-IκBα	21−44	KKERLLDDRH**DSGLDS**MKDEEYEQ
22P-Vpu	41−62 (*20*)	LIDRLIERAE**DSGNES**EGEISA
32P-β-catenin	17−48 (*21*)	DRKAAVSHWQQQSYL**DSGIHS**GATTTAPSLSG

degradation through the ubiquitin-dependent proteasome pathway (*11*) (Figure 1). The role of β-TrCP in the Skp1-Cdc53-F-box protein (SCF) ubiquitin ligase complex is to select and recruit the proper substrate for polyubiquitination by the SCF. This is achieved by the modular organization of β-TrCP, which allows for simultaneous interactions with the target protein on the one hand through its C-terminal WD repeats and the SCF on the other hand through interactions between its F-box domain and Skp1 (*12*). This finding was of particular significance, since there is evidence for the involvement of the ubiquitin−proteasome machinery in Vpu-mediated CD4 degradation (*13*, *14*). The human immunodeficiency virus type 1 (HIV-1) Vpu protein, the first ligand of β-TrCP to be identified (*11*), binds to the CD4 receptor and induces its degradation by cytosolic proteasomes. The important role of β-TrCP in the regulated degradation of cellular proteins was confirmed because β-catenin, as well as IκB-α, is degraded by the proteasome after ubiquitination by SCF−β-TrCP (*15*).

Similar to the β-TrCP-binding domain in Vpu (*16*), the signal for recognition of both IκB and β-catenin by β-TrCP includes a pair of conserved phosphorylated serine residues that are arranged in a consensus motif, DS[PO_3^{2-}]G**X**XS[PO_3^{2-}] (where **X** represents a hydrophobic residue) present in all three proteins. Serine phosphorylation plays a major role in regulating the stability of SCF target proteins. In the case of IκB-α, activation of the IκB kinase complex following stimulation by cytokines such as TNF-α results in the phosphorylation of two serine residues (Ser32 and Ser36) and leads to the rapid degradation of IκB-α by cytosolic proteasomes (*1*, *17*) (Figure 1).

The SCF−β-TrCP complex specifically recognizes a Vpu peptide fragment of 22 amino acids (*18*), the 22P-Vpu peptide; a 19-amino-acid motif in IκB-α; and a 22-residue β-catenin polypeptide in a phosphorylation-dependent manner (*19*). To elucidate the basis of β-TrCP recognition, the bound structures of the 22P-Vpu$^{41-62}$ (*20*) and 32P-β-Catenin (*21*) peptides to the F-box protein β-TrCP were previously determined by using NMR and MD. Recently, it was shown that Vpu is resistant to β-TrCP-mediated degradation and that it competitively inhibits β-TrCP-dependent degradation of IκB-α in response to tumor necrosis factor-α (TNF-α), resulting in the suppression of NF-κB activity in Vpu-expressing cells (*22*, *23*). This work is a continuation to elucidate a three-dimensional structure of β-TrCP ligands and also describes attempts to correlate structures with biological activity. The results obtained for compounds Vpu (*20*) and β-Catenin (*21*) were then compared with the conformational behavior of IκB-α as described in the following.

To better understand the interaction of IκB-α with β-TrCP, we subjected a 24-residue phosphorylated peptide (hereafter referenced as 24P-IκBα, Table 1) to detailed conformational analyses in the free state and when it was bound to β-TrCP protein. First, we have investigated the solution conformation of 24P-IκBα by CD and NMR spectroscopies. The NMR study in phosphate-buffered saline solution was coupled with molecular modeling to determine precisely the conformation of 24P-IκBα and to examine the structural influence of phosphorylation at the two sites Ser32 and Ser36 of the free 24P-IκBα. Then, we report the β-TrCP-bound conformation of 24P-IκBα and characterize the binding process by NMR methods. Transferred nuclear Overhauser enhancement (TR-NOE) spectroscopy is successfully applied to investigate the conformation of a ligand in its bound form (*24*, *25*). TRNOESY experiments were further completed by molec-

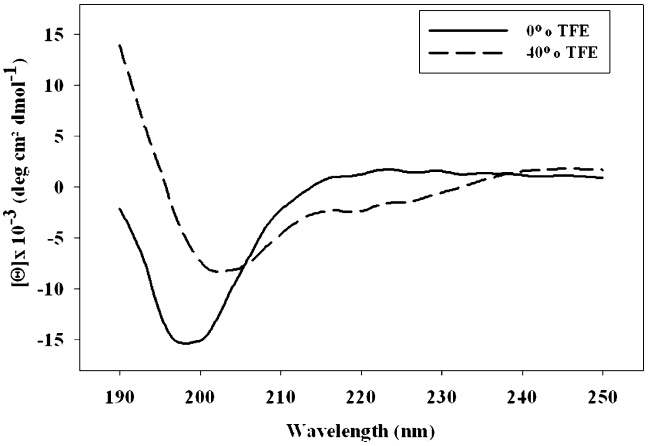

FIGURE 2: CD spectra of 24P-IκBα at 280 K in PBS solution at pH 7.2 and in 40% (v/v) TFE/water (− − −).

ular modeling studies to determine the structural properties of the 24P-IκBα peptide bound to β-TrCP. An additional technique, the saturation transfer difference (STD) NMR method, allows determination of binding epitopes (*26*, *27*) of the 24P-IκBα peptide.

MATERIALS AND METHODS

Peptide Synthesis. IκB-α fragment (*21*−*44*) hereafter referred to as peptide 24P-IκBα was purchased from NeoMPS Lab., Strasbourg, France. The amino acid sequence is (Ac-Lys^{21}−Lys−Glu−Arg−Leu−Leu−Asp−Asp−Arg−His−Asp−Ser(PO_3H_2)−Gly−Leu−Asp−Ser(PO_3H_2)−Met−Lys−Asp−Glu−Glu−Tyr−Glu−Gln^{44}-NH_2) for the peptide containing the phosphorylated sites 32 and 36, Ser(PO_3H_2). The purity (95%) of the peptides was tested by analytical HPLC and by mass spectrometry.

Purification of the WD Repeat Region from Human Protein β-TrCP. The β-TrCP protein was expressed as a fusion protein with glutathione *S*-transferase (GST). The previously described construction (*11*) resulted in a fusion protein of ~60 kDa corresponding to the 218 residues of the GST, an 18-mer linker, and the seven WD repeats (residues 251−569) of β-TrCP, hereafter named GST-β-TrCP. The expression, separation, and purification of GST-β-TrCP were accomplished following a standard GST fusion protein protocol that was previously described (*20*). The purified recombinant protein was then used to prepare the NMR samples.

Circular Dichroism Spectroscopy. CD spectra were recorded at 20 °C from 250 to 190 nm on a Jasco model 710 spectropolarimeter, using cells with 1 mm path length (Figure 2). A stock solution of 5 mM peptide dissolved in 5 mM phosphate buffer was used to prepare CD samples in water or water/organic mixtures. The spectra were measured at peptide concentrations of 20 μM. The ellipticity is reported as mean residue molar ellipticity at 222 nm, Θ_{222}, in deg cm^2 dmol^{-1}. Samples were scanned over the wavelength range 202−250 nm by recording values every 0.1 nm with 50 nm min^{-1} scan rate, with an integration time of 2 s and a 2 nm bandwidth. Each spectrum was the average of four scans. The secondary structure percentage predictions were made using CDNN software (http://www.imtech.res.in/pub/pspt/cdnn/).

NMR Spectroscopy. All NMR experiments were recorded on an Avance 500 NMR spectrometer (Bruker Biospin, Wissembourg, France) equipped with a Bruker TXI triple resonance probe including shielded *z*-gradients. Two 0.5 mL 24P-IκBα samples were used at pH 5.4 and 7.2: a 2 mM aqueous sample containing 90% H_2O/10% D_2O, with 20 mM sodium phosphate buffered solution and 0.02% NaN_3. Temperature was set at 280, 293, and 303 K in water. NMR samples contained nonphosphorylated 24-IκBα or phosphorylated 24P-IκBα with or without the GST−β-TrCP protein. They were prepared in phosphate-buffered saline solution, pH 7.2 (20 mM phosphate, 5% D_2O, 0.02% NaN_3). ^{1}H NMR spectra were recorded at constant temperature (280 K). The NMR samples were adjusted to a protein concentration of 0.01 mM based on the visible absorption at 595 nm. A 200-fold ligand excess (2 mM) over binding sites was used throughout the studies. The following conventional two-dimensional experiments were carried out: 2D TOCSY (*28*), NOESY (*29*), ^{1}H−^{13}C HSQC (*30*), and ^{1}H−^{13}C HMBC (*31*). TOCSY spectra were acquired with a 80 ms spin-lock time using a MLEV-17 sequence in water (*32*). NOESY spectra were recorded with mixing times from 100 to 600 ms and TRNOESY with mixing times from 50 to 300 ms. TOCSY, NOESY, and HSQC experiments were performed in the phase-sensitive mode, using the time-proportional phase incrementation method for quadrature detection (TPPI or States-TPPI) (*33*). For the TOCSY and NOESY experiments, water suppression was achieved using the pulsed-field gradient-based Watergate method (*34*). For the heteronuclear experiments performed in aqueous solution, water resonance was suppressed with a low-power presaturation. The spectra were recorded with 512(t_1) × 4096(t_2) data points and with a proton spectral width of 5555.6 Hz in water and a carbon spectral width of 22 639.3 Hz. Two-dimensional TRNOESY experiments were recorded with a total of 512(t_1) × 4096(t_2) data points for each experiment. The total relaxation delay was 1.5 s. Mixing times of 100, 200, and 500 ms were utilized. The sample was prepared with 0.25 mg of GST−β-TrCP protein (0.01 mM protein) and 3.1 mg of the 24P-IκBα peptide (2 mM; 200:1 peptide/binding site ratio) in 500 μL of buffer. The interproton distances were obtained from volume integrals employing HA and HB of Tyr42 as a reference spin pair and a distance approximation of 2.43 Å between the two-aromatic protons. Data were processed on a Silicon Graphics Indigo 2 or O2 workstation using XWIN−NMR. The observed NOE correlations were assigned and integrated using FELIX software (Accelrys). The t_1 dimension was generally zero-filled to 1024 real data points with the t_1 and t_2 dimensions being multiplied by shifted sinebell functions prior to Fourier transformation. In water, proton chemical shifts were reported relative to TSP-d_4, 3-(trimethylsilyl)[2,2,3,3-d_4] propionic acid, sodium salt (Tables 2 and 3), and the ^{13}C chemical shifts were referenced indirectly using TSP-d_4 taken as reference. The sequential assignment of the peptide was performed using the standard sequential assignment strategy (*35*).

For 1D STD experiments (*26*), saturation transfer was achieved by using a series of 40 equally spaced 50 ms Gaussian-shaped pulses for selective saturation (then, total saturation time was approximately 2.0 s) (*36*), with 1 ms delay between the pulses. With an attenuation of 50 dB, the radiofrequency field strength for the selective saturation

pulses in all STD NMR experiments was 190 Hz. The irradiation yields full saturation of the protein by efficient spin diffusion. For one set of spectra, the protein envelope was irradiated at −2 ppm (on-resonance) and 30 ppm (off-resonance) showing that by irradiating at $\delta = -2$ ppm, the entire protein can be saturated uniformly and can therefore be efficiently used for the STD NMR technique. Setting the on-resonance frequency to 11 ppm generated another set of spectra. For the on-resonance irradiation frequency, values around −2 ppm are practical because no ligand nuclei resonances are found in this spectral region whereas the significant line width of protein signals still allows selective saturation. Investigation of the time dependence of the saturation transfer with saturation times from 0.2 to 4.0 s showed that 2 s was needed for efficient transfer of saturation from the protein to the ligand protons. Subtraction of FID values with on- and off-resonance protein saturation was achieved by phase cycling. Because no baseline distortion was observed, no $T_1\rho$ filter was applied to eliminate the background resonances of the GST−β-TrCP protein. A total relaxation delay (Aq + d_1) of 3.4 s and eight dummy scans were employed to reduce substraction artifacts. One thousand total scans (or 10 000 for a better signal-to-noise ratio) were collected. One-dimensional spectra were multiplied with exponential functions (LB = 2 Hz) and zero-filled two times. Relative STD values were calculated by dividing STD signal intensities by the intensities of the corresponding signals in a 1D ^{1}H NMR reference spectrum of the same sample recorded with 512 scans and similarly processed. For STD experiments, the ligand to protein ratio was set to 200:1 (2 mM 24P-IκBα peptide, 0.01 mM GST−β-TrCP protein).

For STD NMR experiments, the following control experiments have been performed.

(i) Samples containing only the ligand molecules were subjected to one-dimensional STD NMR experiments using saturation conditions identical to those applied in the one-dimensional STD NMR experiments with the ligands in the presence of GST−β-TrCP. The resulting difference spectra did not contain any signals, showing that saturation transfer via the protein was the sole reason for the effects observed using samples with the ligand molecules in the presence of GST−β-TrCP.

(ii) One-dimensional STD NMR experiments were performed with 24P-IκBα and other fusion proteins such as GST−N-Ter, which corresponds to the GST protein fused with the first 260 residues of the full-length β-TrCP protein, including the F-Box but not the WD domains. The resulting one-dimensional spectra contained no signals, demonstrating the specificity of the interaction observed between 24P-IκBα and the GST−β-TrCP fusion protein. The sample control was prepared containing the 24P-IκBα phosphorylated peptide with the GST−N-Ter protein at the same ratio 200:1 as that used for the 24P-IκBα/GST−β-TrCP sample.

Three-Dimensional Structure Calculation. Distance restraints for 24P-IκBα structure calculation were derived from NOE cross-peaks in the NOESY spectrum recorded at 298 K with τ_m = 500 ms and in the TRNOESY spectrum recorded at 298 K with τ_m = 200 ms that were converted into distances by volume integration using the FELIX software. The NOE intensity between the Tyr42 aromatic protons, which corresponds to a distance of 2.43 Å, was used for calibration.

The final list of distance restraints containing 247 restraints from the NOESY and 317 restraints from the TRNOESY spectra was incorporated for structure calculation with the standard protocol of ARIA 1.2 (*37*, *38*) using a simulated annealing protocol. By default, ARIA calibrates distance restraints by computing the relaxation matrix from the NOE peak volumes and the chemical shift assignments (*39*). The starting point for ARIA is an almost complete assignment of the proton chemical shifts, and a list of partially assigned NOEs, mostly sequential and secondary structure NOEs. The restraint list is then augmented by automatically interpreting peak lists generated by automated peak-picking (*40*). A force field adapted for NMR structure determination (the PARALLHDG 5.3 parameters file) was used. A rotational correlation time of 2 ns for the free peptide and 8 ns for the peptide bound to the GST−β-TrCP protein was used for computation of the relaxation matrix. Starting from an extended conformation with random side chain conformation, the simulated annealing protocol consisted of four stages: a high temperature torsion angle simulated annealing phase at 10 000 K (30 ps), a first torsion angle dynamics cooling phase from 10 000 to 50 K (15 ps), a second Cartesian dynamics cooling phase from 2000 to 50 K (27 ps), and a final minimization phase at 50 K. ARIA runs were performed using the default parameters with eight iterations. Twenty structures were generated each round, and the 10 lowest-energy structures were carried to the next iteration. Nevertheless, some ambiguous assignments still remained and were introduced with an appropriate treatment in ARIA (*40*). The central task of ARIA is the assignment of ambiguous NOEs during the structure calculation using a combination of ambiguous distance restraints and an iterative assignment strategy. In addition, ARIA calibrates ambiguous NOEs to derive distance restraints, merges overlapping data sets to remove duplicate information, and uses empirical rules to identify erroneous peaks (*41*). A set of 60 structures was then generated. The residues, except the N-Ter Lys21, Gly33, and Gln44, were constrained using 21 ϕ dihedral angles constraints between −20° and −180° (usually the only range considered in NMR-derived structures), the region of a Ramachandran plot populated by nearly all nonglycyl residues. While ARIA allows the final free structures to undergo a procedure in a simulated water box, it was decided that this step was not applicable for the bound peptide in the hydrophobic recognition sites. After the final iteration with ARIA software (OPLS force field), 20 structures were generated, and the 10 best with lower energies were retained as the final structures. The final list of distant restraints contained 247 restraints for the free peptide, divided into 136 intraresidue, 96 sequential, 13 medium-range, and 2 long-range NOEs and 317 restraints for the bound peptide, divided into 166 intraresidue, 92 sequential, 36 medium-range, and 23 long-range NOEs. Analysis of the ARIA results (Table 4) was carried out using the overview.aria script (*42*). The final PDB structures were analyzed and visualized with PROCHECK-NMR (*43*) and MOLMOL (*44*) programs. The resultant structures were subjected to a check of NOE distance violation of >0.3 Å from the observed distances. The set of 24P-IκBα structures was selected for structural analysis according to good geometry and few NOE violations and by eliminating those structures with ϕ, ψ values in the

Table 2. ^{1}H and ^{13}Cα NMR Chemical Shifts of the Free Peptide 24P-IκBα in ppm from TSP-d_4,[a] and Amide Signal Shift Temperature Coefficients ($\Delta(\delta$ NH)/ΔT in ppb K^{-1}

residue	NH	CαH	Cβ H	other	$\Delta(\delta$ NH)/ΔT	^{13}Cα
Lys21	NH_3^+	4.04	1.94	Cγ H 1.44; Cδ H 1.67/1.71; Cε H 3.00	*b*	54.0
Lys22	*b*	4.36	1.81	Cγ H 1.45; Cδ H 1.66/1.78; Cε H 3.01	*b*	54.6
Glu23	8.76	4.28	1.94/2.08	Cγ H 2.25/2.33	−6.5	54.5
Arg24	8.62	4.36	1.79/1.85	Cγ H 1.63; Cδ H 3.19; Nε H 7.44	−8.9	54.5
Leu25	8.65	4.37	1.63/1.68	Cγ H 1.61; Cδ H 0.87/0.94	−9.3	53.6
Leu26	8.43	4.29	1.64/1.69	Cγ H 1.61; Cδ H 0.88/0.94	−8.7	54.3
Asp27	8.33	4.59	2.69/2.77		−6.5	52.8
Asp28	8.19	4.59	2.61/2.72		−2.1	52.8
Arg29	8.30	4.32	1.79/1.86	Cγ H 1.62; Cδ H 3.21; Nε H 7.53	−7.1	54.5
His30	8.72	4.69	3.19/3.31	4H 7.24; 2H 8.49	−7.6	54.1
Asp31	8.67	4.65	2.63/2.71		−9.3	52.6
pSer32	9.18	4.46	4.13		−8.5	56.8
Gly33	8.66	3.92; 4.07			−4.2	44.3
Leu34	8.04	4.41	1.67/1.69	Cγ H 1.61; Cδ H 0.88/0.94	−4.1	53.4
Asp35	8.39	4.61	2.64/2.75		−5.7	52.8
pSer36	9.00	4.34	4.09		−8.5	56.8
Met37	8.65	4.44	2.04/2.12	Cγ H 2.58/2.61; Cε H 2.13	−7.0	54.1
Lys38	8.40	4.37	1.77/1.86	Cγ H 1.42; Cδ H 1.70; Cε H 3.01	−6.6	54.6
Asp39	8.56	4.59	2.60/2.75		−7.5	52.9
Glu40	8.54	4.25	1.92/2.04	Cγ H 2.23/2.28	−8.3	55.0
Glu41	8.49	4.24	1.88/1.98	Cγ H 2.14/2.24	−6.3	55.1
Tyr42	8.22	4.60	2.94/3.06	CdH 7.13; CeH 6.82	−6.9	56.2
Glu43	8.44	4.28	1.90/2.05	Cγ H 2.22/2.27	−7.5	54.9
Gln44	8.13	4.12	1.94/2.15	Cγ H 2.30/2.32; Nε H 6.94/7.67	−6.6	55.9

[a] Spectra were recorded at 280 K, pH 7.2, and 20 mM sodium phosphate buffer; $H_2O/^2H_2O$, 9:1 (by volume). [b] Resonances of protons were not determined.

disallowed regions of the Ramachandran plot specified with Procheck.

The crystal structure of β-TrCP−SkP1protein−β-catenin ligand complex (*45*) from the PDB were used to generate a separate set of coordinates for the whole protein, its β-catenin ligand, and the corresponding active site. The input conformation of the ligand was directly extracted from the X-ray structure. The X-ray ligand of the complex was considered as the bioactive structure and can be further used as the reference to evaluate computed conformations from NMR bound peptides (24P-IκBα, β-catenin, and Vpu). No energy minimization of the ligand was performed. The β-TrCP protein active site was defined as the collection of amino acids for which at least one atom is nearer than 6 Å to any atom of the bound ligand. Superimposition of the lowest energy structure of the bound 24P-IκBα peptide and the crystal structure was performed from residues 31 to 34, essentially for the D**pS**GX region of the consensus D**pS**-GXX**pS** motif. Comparison is based on shape complementary but also favorable ligand−receptor interactions; the results are also examined with regard to the polar as well as hydrophobic surface area of the ligands.

RESULTS

CD Spectroscopy. In order to determine more favorable conditions for further structural analysis, CD spectra of 24P-IκBα were recorded in different media. The PBS solution of 24P-IκBα at pH 7.2 was titrated with TFE from 0 to 50% (v/v). As shown in Figure 2, the CD spectra obtained in aqueous buffered solution indicated the absence of regular secondary structure. 24P-IκBα exhibited a negative band around 200 nm and a positive band around 220 nm indicating the possibility of a random coil structure. Addition of trifluoroethanol to solution did not change the CD spectra of 24P-IκBα drastically. The addition of TFE results in a nascent helical conformation in the solution containing 40% TFE (v/v).

For the same peptide at pH 5.4, the results are somewhat similar. The shape of the curves indicates the presence of some secondary structure in the peptide, but the propensity of helical parts to increase when TFE is added seems less clear, which suggests that protonation of pSer32, pSer36, and His30 destabilizes the secondary structure adopted by the peptide at pH 7.2. For this reason, and because a phosphate-buffered solution at pH 7.2 reproduces better the physiological conditions under which 24P-IκBα is stable, the NMR and structural study of the phosphorylated peptide has been followed at this pH.

The CD spectra showed very similar curves for temperatures between 7 and 30 °C, suggesting no real differences for the two peptides under these conditions of temperature.

NMR Spectroscopy. The ^{1}H resonances of 24P-IκBα in PBS at pH 7.2 were determined by a series of TOCSY (*28*) and NOESY (*29*) experiments. The ^{13}Cα signals were assigned using ^{13}C-edited HSQC (*30*) and HMBC (*31*) experiments on a ^{13}C natural abundance sample. Proton resonances of 24P-IκBα in buffer at 280 K are reported in Table 2. TOCSY spectra were used to assign spin systems of most of the amino acid residues, and NOESY data provided the sequential connections between these spin systems. The aromatic side chains were identified using ^{13}C-edited HSQC and HMBC experiments on a ^{13}C natural abundance sample and the NOE connectivities between Cβ protons and aromatic ring protons. The chemical shift data for 24P-IκBα bound to β-TrCP protein are shown in Table 3. The Hβ protons of pSer32 and -36 residues were well separated indicating a more stable side chain conformation of pSer32 and -36 in 24P-IκBα bound peptide.

A first assessment of secondary structural features was obtained by analyzing 24P-IκBα ^{1}Hα and ^{13}Cα chemical

Table 3. ^{1}H NMR Chemical Shifts of the Mixture of 2 mM 24P-IκBα Peptide and 0.01 mM GST−β-TrCP Protein in ppm from TSP-d_4[a]

residue	NH	CαH	CβH	other
Lys21	NH_3^+	3.99	1.87/1.91	CγH 1.42/1.45; CδH 1.70; CεH 3.01
Lys22	*b*	4.34	1.74/1.81	CγH 1.42/1.47; CδH 1.72; CεH 3.00
Glu23	8.75	4.28	1.93/1.98	CγH 2.25/2.29
Arg24	8.62	4.36	1.79/1.85	CγH 1.61/1.62; CδH 3.18; NεH 7.43
Leu25	8.65	4.38	1.67/1.69	CγH 1.58; CδH 0.87/0.94
Leu26	8.42	4.30	1.67	CγH 1.61; CδH 0.88/0.93
Asp27	8.32	4.59	2.68/2.74	
Asp28	8.19	4.58	2.68/2.75	
Arg29	8.29	4.30	1.77/1.86	CγH 1.59/1.64; CδH 3.20; NεH 7.52
His30	8.68	4.67	3.17/3.24	4H 7.17; 2H 8.34
Asp31	8.60	4.63	2.60/2.70	
pSer32	9.20	4.45	4.10/4.13	
Gly33	8.66	3.92; 4.05		
Leu34	8.03	4.41	1.63/1.68	CγH 1.56; CδH 0.86/0.92
Asp35	8.38	4.63	2.62/2.74	
pSer36	9.07	4.43	4.03/4.08	
Met37	8.67	4.45	2.02/2.11	CγH 2.56/2.60; CεH 2.09
Lys38	8.41	4.35	1.77/1.81	CγH 1.42; CδH 1.65; CεH 2.99
Asp39	8.55	4.60	2.59/2.73	
Glu40	8.54	4.24	1.91/2.07	CγH 2.21/2.26
Glu41	8.49	4.24	1.89/1.94	CγH 2.15/2.21
Tyr42	8.22	4.62	2.94/3.06	CdH 7.13; CeH 6.81
Glu43	8.44	4.28	1.91/2.08	CγH 2.22/2.26
Gln44	8.12	4.11	1.93/2.16	CγH 2.29/2.34; NεH 6.94/7.66

[a] Spectra were recorded at 280 K, pH 7.2, 24P-IκBα/β-TrCP = 200 (2 mM 24P-IκBα peptide, 0.01 mM GST−β-TrCP protein), and 20 mM sodium phosphate buffer; $H_2O/^2H_2O$, 9:1 (by volume). The chemical shifts are the averages of those of the bound peptide and the peptide excess. [b] Resonances of protons were not determined.

Table 4. Structural Statistics of the Final 20 NMR Structures of 24P-IκBα Free and 24P-IκBα Bound to the β-TrCP Protein

	$ARIA_{output}$	
	24P-IκBα free	24P-IκBα bound
No. of Exptl. Distance Restraints		
unambiguous NOE	201	313
ambiguous NOE	46	4
total NOEs	247	317
Divided into		
intraresidue NOE	136	166
sequential NOE	96	92
medium-range NOE	13	36
long-range NOE	2	23
no. of exptl. broad dihedral restraints	21	21
NOE violations >0.3 Å per structure	1.8	0.5
rmsd[a] (Å) to a Mean Molecule		
backbone (all residues)	5.46 ± 1.52	1.33 ± 0.38
heavy atoms (all residues)	6.86 ± 1.54	2.63 ± 0.63
backbone (residues 25−40)	3.37 ± 1.03	0.93 ± 0.40
heavy atoms (residues 25−40)	4.86 ± 1.14	1.90 ± 0.60
backbone (residues 22−31)	1.75 ± 0.58	0.60 ± 0.22
heavy atoms (residues 22−31)	3.39 ± 0.77	1.91 ± 0.52
backbone (residues 30−36)	1.50 ± 0.38	0.63 ± 0.29
heavy atoms (residues 30−36)	3.43 ± 0.71	1.68 ± 0.48
Ramachandran Plot of Residues[b] (%)		
in most favored regions	55	52
in additional allowed regions	43.1	44
in generously allowed regions	1.7	4
in disallowed regions	0.2	0

[a] Calculated by MOLMOL. [b] Calculated by PROCHECK.

shifts because their deviations from the random coil values are representative of peptide/protein secondary structure (*46*). The proton and carbon variations observed were less than 0.1 and 1 ppm, respectively, which reflects a predominantly random conformation in water. Nevertheless, in the bound states, residues 23−25 and 27−29 had low frequency α proton and high-frequency carbon chemical shifts differing from the random coil values by more than −0.05 and 0.2 ppm, respectively, suggesting the presence of a nascent helix between residues 23 and 29.

The dissociation constant was measured for the interaction of the phosphorylated 24P-IκBα peptide with the GST−β-TrCP protein. The interaction caused environmental changes on the peptide protein interfaces and hence, affected the chemical shifts of the nuclei in this area. We followed the NH resonances to their bound position, and we extracted the binding constant by fitting the fractional shift against an equation depending on total GST−β-TrCP protein and 24P-IκBα concentrations (*47*, *48*). The K_d was estimated around 500 μM and was characteristic of fast exchange conditions.

Temperature dependence of amide proton chemical shift showed that the amide of Asp28 has a temperature coefficient of chemical shift of -2.1×10^{-3} ppm/K. Other amide protons in the peptide (Gly33, Leu34, and Asp35) showed $\Delta\delta/\Delta T$ values in the range of $(-4 \text{ to } -6) \times 10^{-3}$ ppm/K. These data suggested that Asp28, Gly33, Leu34, and Asp35 are intramolecularly hydrogen bonded or solvent shielded.

After a NOE buildup analysis, a mixing time of 500 and 200 ms was used for the free and for the bound peptide, respectively (*49*). At the 200 ms mixing time, there is no spin diffusion in the TRNOESY. The free peptide showed very poor NOESY spectra at this mixing time. The free peptide could be flexible in solution only showing sequential NOEs; the inter-residue NOEs could be observed at mixing times higher that 200 ms. When we increased the mixing time to 500 ms, we were able to detect some NOE cross-peaks, both short-range and long-range. The addition of β-TrCP protein could be stabilizing some structure and decreasing the tumbling rate. The total number of assigned NOEs varied from 201 to 313 (Table 4). Figure 3 summarizes the structural features observed for the free and bound 24P-IκBα peptide.

Most of the NOEs for the free peptide were intraresidue and sequential (Figure 3A). The free peptide showed only two long-range NOEs and 13 medium-range NOEs, suggesting that the free peptide behaves as a random coil in solution, not showing any structural tendency. Interestingly, there are no $d_{\alpha N}(i,i+2)$ connectivities observed in the region containing the ^{31}D**pS**GXX**pS**^{36} motif, for the free 24P-IκBα, but two Hα−HN NOEs (25−27 and 26−28) are present in the N-terminal region and two Hβ−HN NOEs (38−40 and 40−42) in the C-terminal region. This suggests that this central region containing the ^{31}D**pS**GXX**pS**^{36} motif is less compact, probably due to the phosphate groups, which could be pushed back. Interestingly, in the 30−40 region containing the DSGXXS motif, there is one long-range connectivity observed for the side chain protons of His30 and Lys38, suggesting that the side chains are constrained. As a consequence, the free 24P-IκBα seems to be only poorly folded with a tendency to form a large bend. This qualitative interpretation of the NOE data is in agreement with the result of structure calculations.

FIGURE 3: Summary of the sequential $d(i,i+1)$ and medium-range $d(i,i+2)$ and $d(i,i+3)$ NOEs used for secondary structure determination of 24P-IκBα (A) free in PBS solution and (B) bound to β-TrCP. After optimization of the 24P-IκBα peptide/protein ratio, the final sample was prepared with 0.25 mg of GST−β-TrCP protein (0.01 mM protein) and 3.1 mg of the 24P-IκBα peptide (2 mM; 200:1 peptide/binding site ratio) in 500 μL of buffer. The NOEs are classified into three categories (strong, medium, and weak) based on the cross-peak volumes. The intensity is indicated by the thickness of the bars.

The bound 24P-IκBα peptide, on the other hand, showed 36 medium- and 23 long-range TRNOEs. The important constraints to define a structural tendency could be noted in Figure 3B. The $d_{\alpha N}(i,i+3)$ and $d_{\beta N}(i,i+3)$ connectivities from Gly33 to Ser36 along with amide−amide NOE between ^{31}D**pS**GLD**pS**MK^{38} suggests a large bend conformation around the residues Asp31-pSer32-Gly33-Leu34-Asp35-pSer36-Met37-Lys38. A great number of long-range NOEs were also observed in this central region containing the DSGXXS motif when the phosphorylated peptide was bound to GST−β-TrCP. TRNOESY connectivities between side chain protons of the Asp28 or Arg29 residues and the main backbone (pSer36 or Asp39) appeared upon addition of GST−β-TrCP. The cross-peak pattern shown in Figure 3B indicated a helix tendency between residues 25 and 30. There were medium-range NOE connectivities $d_{NN}(i,i+3)$ between the amides of Leu26−Arg29 and Asp27−His30, as well as long-range NOEs between the side chain protons of other residues (24−29 and 21−28) indicating the helical conformation in the peptide. Besides, the observation of sequential $d_{NN}(i,i+1)$ NOEs, as well as $d_{\alpha N}(i,i+2)$, $d_{\beta N}(i,i+2)$, $d_{\gamma N}(i,i+2)$ and $d_{\beta N}(i,i+3)$, $d_{\delta N}(i,i+3)$, $d_{\epsilon N}(i,i+3)$, and $d_{\delta N}(i,i+4)$ medium-range NOE cross-peaks in the N-terminal domain (Lys22−Asp31) suggested the possible existence of a nascent helix in this region of the peptide. In the C-terminal region, a succession of $d_{NN}(i,i+2)$ and $d_{\alpha N}(i,i+2)$, as well as $d_{\alpha N}(i,i+3)$, $d_{\alpha\beta}(i,i+3)$, and $d_{\beta\gamma}(i,i+3)$, was shown. This observation also suggested the presence of a nascent helix between residues 37 and 42 in the C-terminal domain of 24P-IκBα, as confirmed by the presence of long-range NOEs between side chain protons Hβ of Asp35 or Met37 residues and the main backbone protons HN of Glu43 or Hα of Gln44 residues, as well as between the side chain protons of Asp35 and Gln44 residues.

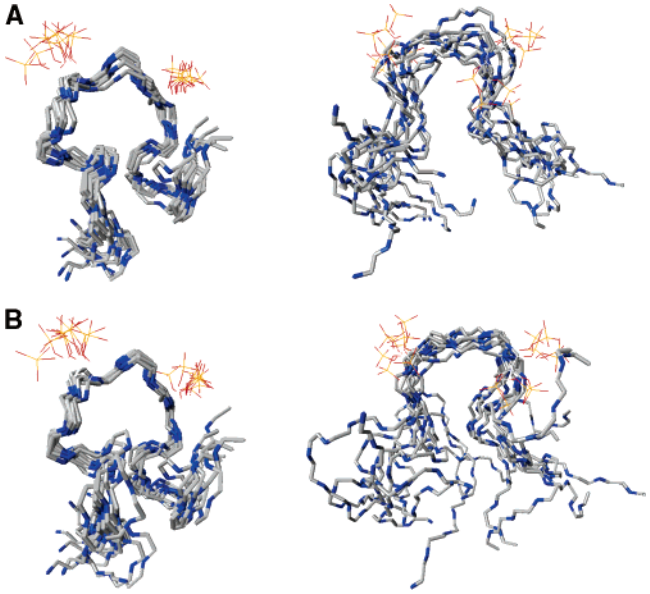

FIGURE 4: TRNOE-derived structure of the 24P-IκBα peptide. Twenty structures were generated with ARIA, and the 10 final structures are displayed bound to β-TrCP (on the left) and free in PBS solution (on the right): (A) superimposition from residue 23 to residue 44; (B) superimposition from residue 30 to residue 36.

Thus, the bound peptide contains a bend at ^{31}D**pS**GLD**pS**MK^{38}. Moreover, bound 24P-IκBα peptide exhibits helical or turn structure at the two Lys22−Asp31 and Met37−Tyr42 regions. The detailed conformational studies were done using molecular dynamics and energy minimization studies using NMR constraints.

Structure of 24P-IκBα. Using NMR data of the 24P-IκBα peptide free in PBS and bound to β-TrCP protein, NOE restrained molecular dynamics and energy minimizations were carried out on the peptide 24P-IκBα using the procedure described earlier. These calculations yielded structures that are consistent with the NMR data. The structure calculation was performed using distance restraints obtained from NOE and TRNOE spectra at 280 K. Among the 20 structures generated from interproton distance restraints with the ARIA protocol in which the 21 available ϕ angle restraints were introduced, 10 exhibited no distance violation larger than 0.3 Å and no ϕ angle violation larger than 10°. Thus, these 10 structures were selected as the final structures. The final structural statistics are given in Table 4, and a superimposition of the backbone atoms (N, Cα, C′) of the final structure ensemble is shown in Figure 4.

Analysis of the geometry violations (Table 4) revealed a good convergence for residues, which confirmed the structural organization of the bound 24P-IκBα (Figure 4B). The

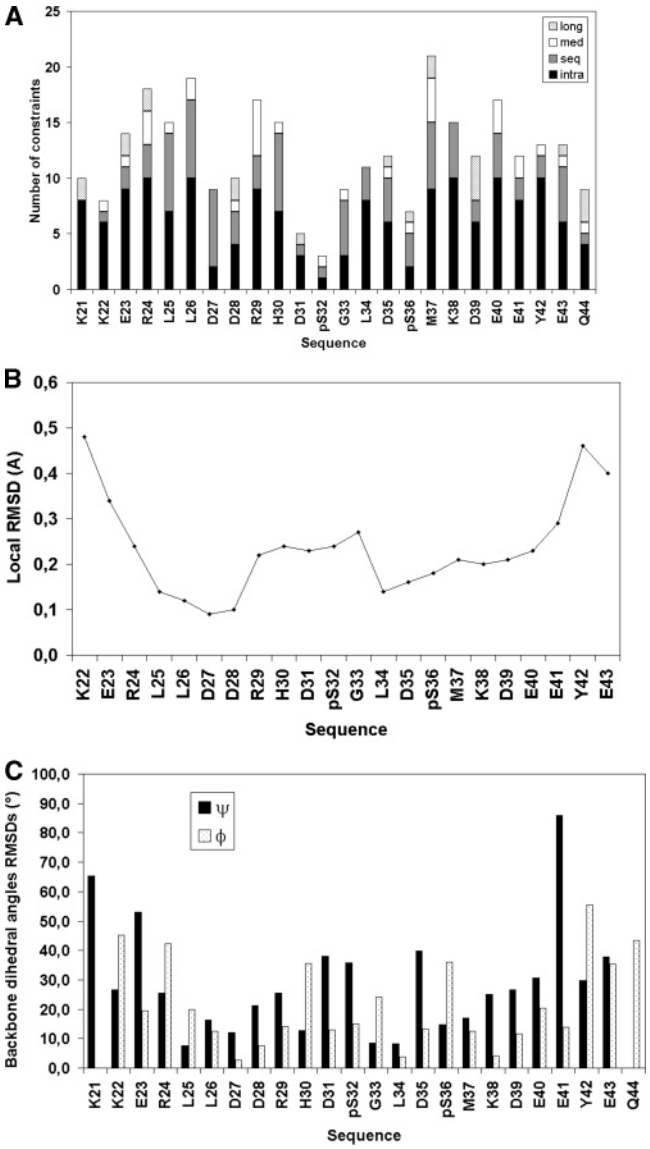

FIGURE 5: Distribution of NOEs and rmsd calculations for 24P-IκBα bound to β-TrCP: (A) distribution of intraresidual (black), sequential (gray), medium-range (white), and long range (dotted) NOEs for each residue; (B) average local rmsd of the backbone atoms from the mean structure upon superimposition of backbone atoms of residues 23−40; (C) backbone dihedral Φ and Ψ angle rmsd values for the 24P-IκBα peptide bound to β-TrCP protein.

structure of the bound 24P-IκBα is composed of a well-defined bend between residues His30 and pSer36, with a low backbone (N, Cα, C′ atoms) rmsd (0.63 Å), Table 4. The bend is flanked by two turn regions, a long one corresponding to the N-terminal residues (Lys22−Asp31) with a low backbone rmsd (0.60 Å), consistent with the number of NOEs per residue observed in this region (average number, 10 NOEs per residue, Figure 5), and a short one corresponding to the C-terminal moiety of the peptide (Met37−Glu43).

Amino acids in the two disordered regions of the free 24P-IκBα (Figure 4A) exhibit high rmsd values (1.50 Å for His30−pSer36 and 1.75 Å for Lys22−Asp31, Table 4) and a lower number of NOEs per residue (average number, 5 NOEs per residue). The well-defined residues were found in the energetically allowed ϕ/ψ space region of the Ramachandran plot (Table 4).

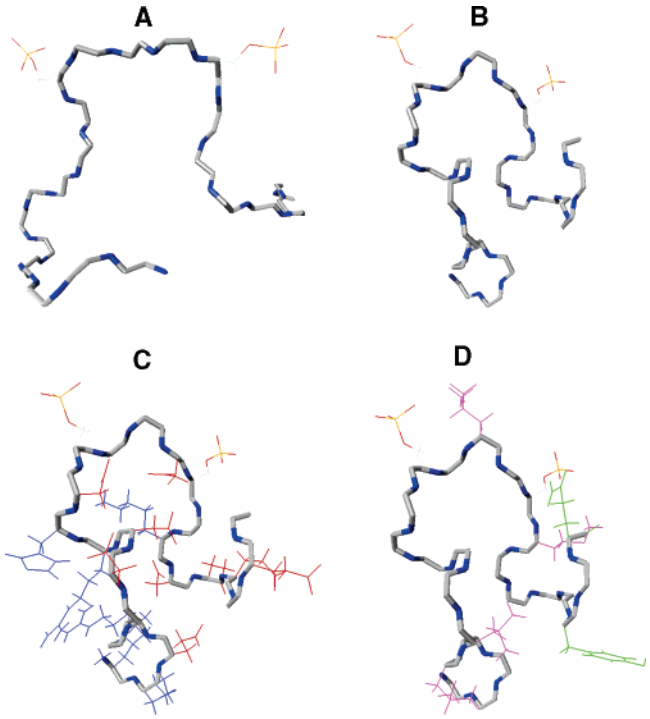

FIGURE 6: A representative structure of (A) 24P-IκBα free in PBS solution and (B) 24P-IκBα bound to β-TrCP, (C) the 24P-IκBα bound structure showing the amphipathicity resulting from the location of negatively charged amino acids in red on one side (Glu23, Glu40, Glu41, Glu43, Asp27, Asp28, Asp31, Asp35, Asp39, **pSer**32, and **pSer**36) and positively charged amino acids in blue on the other side (Arg24, Arg29, His30, Lys21, Lys22, and Lys38), and (D) the structure showing polar (Tyr42, Gln44) and hydrophobic (Leu25, Leu26, Leu34, Met37) amino acids in green and magenta, respectively.

The proposed conformation of 24P-IκBα free and bound obtained from NMR data and MD simulations are shown in Figure 6. The three-dimensional structures of the free and bound 24P-IκBα are not similar. Free 24P-IκBα (Figure 6A) does not acquire stable structure in water although the conformers generated using molecular modeling exhibited only a bend around the residues ^{31}D**pS**GLD**pS**^{36}. The bound peptide presents also a bend corresponding to the ^{31}D**pS**-GLD**pS**^{36} motif but with two turn regions on both sides (Lys22−Asp31 and Met37−Glu43) (Figure 6B). The turn region was stabilized by intramolecular hydrogen bonds involving Arg24, Asp27, Asp28, Arg29, His30, and Asp31. Intramolecular hydrogen bonding was supported by the low-temperature coefficient of chemical shift of Asp28 amide resonance (Table 2). MD simulations and energy minimization data suggested that the C-terminal part of the free peptide is flexible whereas the C-terminal of the bound is stabilized by the intramolecular hydrogen bonds involving Met37, Asp39, Glu41, Tyr42, Glu43, and Gln44. This is consistent with the low local rmsd values (Figure 5b) found for the concerned residues (24−28 and 35−41).

Although no specific restraints (i.e., χ_1 restraints) were used, the side chains adopt a preferential orientation in the backbone. A hydrophilic face contained the positively charged amino acids (Lys21, Lys22, Arg24, Arg29, and His30), and the opposite hydrophilic face presented the negative charged (Asp39, Glu40, Glu41, Glu43) (Figure 6C) and polar (Tyr42, Gln44) amino acids (Figure 6D). The bend shows in an alternate way, the negative charged Asp31 and

pSer32, the hydrophobic residues Gly33 and Leu34, the negative charged Asp35 and pSer36, and the hydrophobic residue Met37 (Figure 6). The model also suggests that the pSer32 and pSer36 phosphate group orientations are different in the two peptides. We have compared the distance between the two phosphorus atoms of pSer32 and pSer36 residues, in the bound 24P-IκBα structures we proposed, as well as of β-Catenin substrate peptides bound to the human β-TrCP−Skp1 complex (*21*, *45*). The peptides are superimposed from residues of the D**pS**GXX**pS** motif at the top face of the β-TrCP WD40 domain (Figure 7). In 24P-IκBα, the average distance between pSer32 and pSer36 was 18.6 Å in the free structures and 15.5 Å in the bound structures. The average distance in β-catenin was 17.1 Å in the crystal structure (*45*) and 15.6 Å in the NMR bound structure (*21*). In Vpu, the distance between pSer32 and pSer36 was 10.2 Å in the NMR bound structure (*20*). The pSer32 and pSer36 residues are placed further apart in 24P-IκBα and β-catenin compared with Vpu due to different folding patterns of the backbones of the three peptides. These structural differences (Figure 7) may play a major role in the selectivity of the β-TrCP receptor for D**pS**GXX**pS** analog peptides.

In conclusion, NMR, CD, molecular dynamics, and energy minimization methods have shown that modification in the D**pS**GXX**pS** motif of β-TrCP ligands leads to different possible structures (Figure 7). These structural differences may be important for the development of β-TrCP receptor selective inhibitors.

Interaction with β-TrCP Protein. The binding of ligands to target molecules can be studied by a variety of NMR methods, depending on the size of the compounds and the kinetics of binding. Current methodology has been reviewed (*36*, *50*). STD is a very sensitive method that allows the mapping of binding epitopes (*27*). Saturation of a single target resonance can result in a rapid spread of saturation over the entire macromolecule if spin diffusion within the macromolecule is efficient. The ligand resonances also become saturated provided that the ligand protons are close in space to the macromolecular protons. The degree of saturation of the individual ligand resonances depends on the binding kinetics and the distance of the protons involved.

The saturation transfer difference (STD) NMR method allows determination of binding epitopes (*26*, *27*) of the 24P-IκBα peptide. This method is based on magnetization transfer by protein signals and their relayed effect to ligand. During the saturation period, progressive saturation transfers from the protein to the ligand protons when the ligand binds to the target. Protons of the ligand that are in close contact with the protein can be identified from the STD NMR spectrum, because they are expected to be saturated to the highest degree. The degree of saturation of individual ligand protons reflects their proximity to the protein surface and can be used as an epitope mapping method to describe the target−ligand interactions (*27*, *51*). The individual signal protons of the 24P-IκBα peptide are best analyzed from the intensity values than the integral values in the reference (I_0) and STD spectra ($I_{STD} = I_0 - I_{sat}$). The spectral region corresponding to the amino protons is well resolved and can be used to classify the amino acid residues relevant for interaction with the β-TrCP protein. The moderate degree of overlapping for the amide protons allowed us to calculate the intensity for all the visible amide protons of the peptide. The signals observed

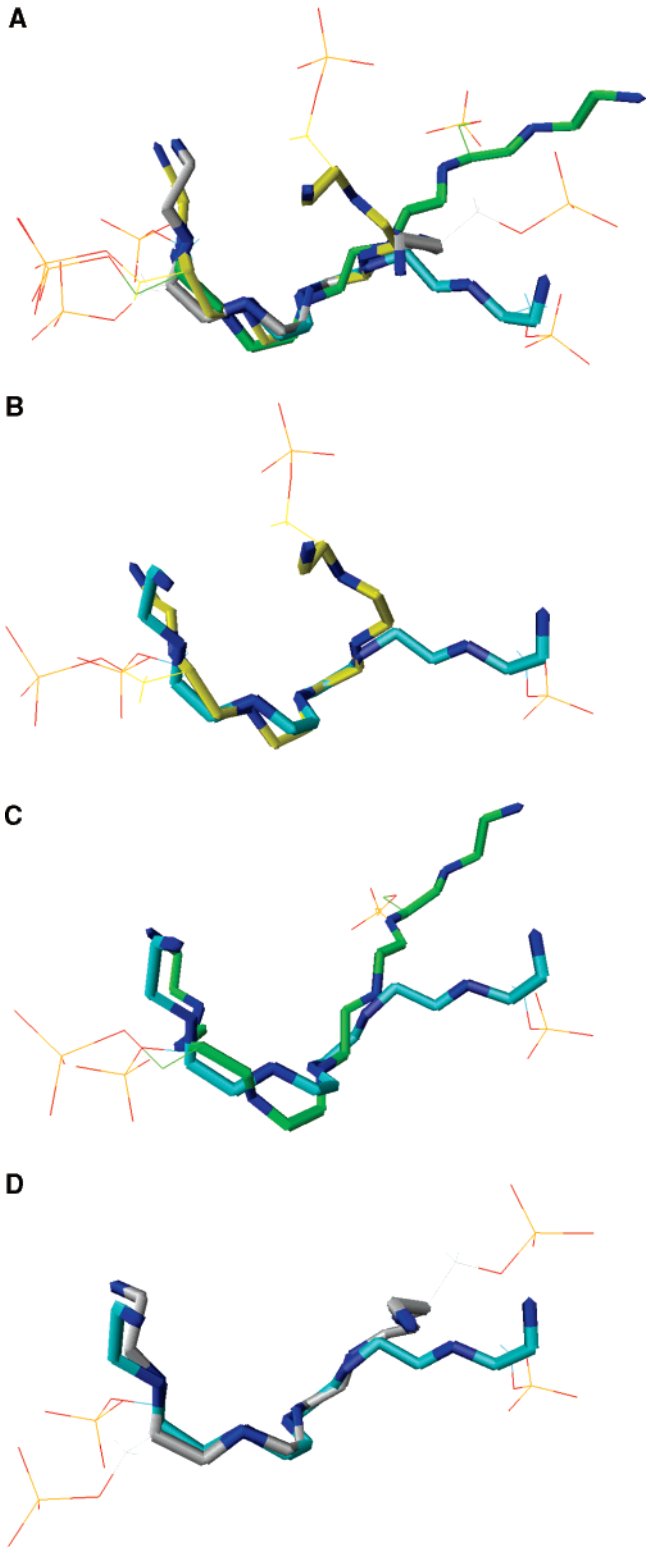

FIGURE 7: The D**pS**GXX**pS** motif where both phosphate groups of phosphoserine are shown and point out of the structures bound to the β-TrCP protein. (A) Superimposition of the D**pS**GXX**pS** fragment for the 24P-IκBα bound peptide (in blue), the NMR Vpu-bound peptide (in yellow) (*20*), the crystal structure of the human β-TrCP−SkP1 complex bound to a β-catenin peptide (in green) (*45*), and the NMR β-catenin-bound structure (in gray) (*21*). The four peptides are superposed from residue D**pS**G. Superimpositions of the D**pS**GXX**pS** fragment for the 24P-IκBα-bound peptide (in blue) and (B) the NMR Vpu-bound peptide (in yellow) (*20*), (C) the crystal structure (in green) (*45*), or (D) the NMR β-catenin-bound peptide (in gray) (*21*).

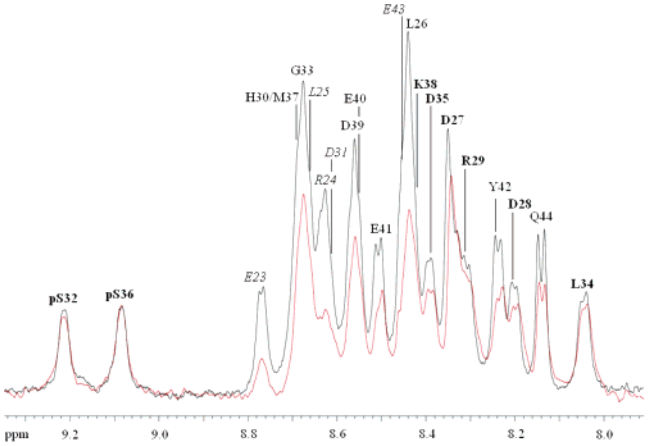

FIGURE 8: Expansion of the region containing resonances of the amide protons of the 24P-IκBα peptide in association with the GST−β-TrCP protein: reference 1D ^{1}H spectrum (in black) and 1D ^{1}H STD-NMR spectrum (in red), showing enhancements of resonances of protons making close contacts with protein interaction site. STD values are obtained after peak picking intensities compared with the 1D with the exact values of chemical shifts of the HN (amino acids in bold have intense relative STD, and those in italic have weak relative STD).

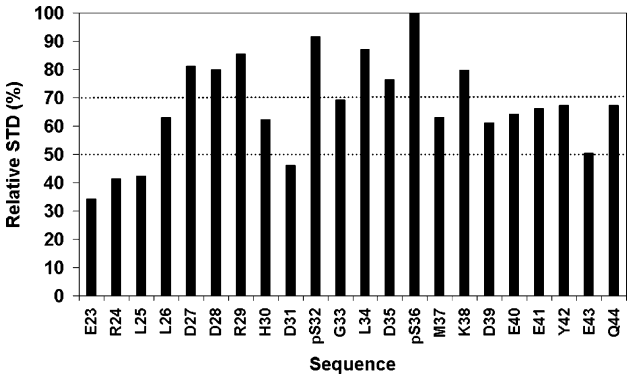

FIGURE 9: Relative STD intensities for 24P-IκBα. The integral value of the largest signal of the 24P-IκBα peptide, the pSer36 HN proton, was set to 100%. The relative degree of saturation for the individual protons normalized to that of the pSer36 can be used to compare the STD effect (*27*). The relative intensities have been classified arbitrarily in three categories (dotted lines).

in the 1D spectra for the amide protons of the whole peptide are summarized in Figure 8.

As a control experiment, we recorded STD−NMR spectra of 24P-IκBα without β-TrCP protein, which confirmed that complex was not formed. The binding of 24P-IκBα to β-TrCP protein was identified by the size and buildup rate of the transferred NOEs combined with STD enhancements (*49*). The STD experiment was initially performed on β-catenin, a peptide ligand for which crystallographic data with β-TrCP are available (*45*).

The signal obtained with the largest I_{STD}/I_0 value, the pSer36 H−N proton, was normalized to 100% (Figure 8). The relative degree of saturation for the individual protons, normalized to that of pSer36, can be used to compare the STD effect (Figure 9). The most prominent STD signals (≥70%) were observed for amide protons HN (pS32−pS36). The closest proximity of this group to the β-TrCP surface might be an indication that this part of the molecule is buried deeper into the β-TrCP ensemble by forming hydrogen bond interactions or involving charged groups. Interestingly, strong enhancements were observed for amide protons of two similar ^{31}D**pS**XXX**pS**^{36} and ^{35}D**pS**XXX**E**^{40} motif (>60%). In the second motif, a glutamic acid residue seems able to replace a phosphorylated serine. On the other hand, amide protons at the ^{25}LLDDRH^{30} fragment have similar larger STD intensities, ranging from 50% to 80%, indicating that these side chains are also involved in the epitope (Figure 9). The STD results highlight the binding of three motifs shown to play a significant role in the stabilization of the complex.

DISCUSSION

HIV-1 Vpu, the first ligand of β-TrCP to be identified (*11*), is a general inhibitor of the degradation of the β-TrCP substrates. Besides serving as an adaptor for CD4 degradation, Vpu is a strong competitor that can inhibit the degradation of the β-TrCP substrates, leading them to accumulate in HIV-1-producing cells expressing Vpu. In fact, IκB-α, β-catenin, and ATF4 accumulate, and the transcriptional activity of β-catenin is up-regulated in the presence of Vpu (*23*). It was also found that β-TrCP is redistributed from the nucleus to the cytoplasm in cells expressing Vpu. The production of Vpu completely prevented the TNF-α-induced nuclear translocation of NF-κB (*23*), as was inhibited NF-κB activity (*22*). Finally, the results suggest that Vpu is a powerful inhibitor of IκB-α degradation and of NF-κB activity (*23*). All these effects require the presence of an intact phosphorylation motif D**pS**GXX**pS** in the cytoplasmic domain of Vpu. This β-TrCP binding site is well conserved in all β-TrCP ligands identified so far (Figures 10 and 11). All these results support a model in which each ligand competes with all other ligands to interact with the same WD repeat domain of β-TrCP (Figure 11), through an analogous phosphorylation motif. Thus, it was interesting to highlight the structural and binding similarities of all SCF−βTrCP substrates.

Three-Dimensional Structures. The characterization of the three-dimensional free and bound structures of 24P-IκBα in solution is an essential step toward the rational design of a selective competitor of its receptor. The identification of β-TrCP protein as the receptor of 24P-IκBα, Vpu (*20*), and β-catenin (*21*) will now allow study of the binding affinity and the functional properties of potential ligands for this receptor. Because structural information for the ligand/receptor complex is currently difficult to obtain, a ligand-based approach can be used to obtain such information. In buffered solution, 24P-IκBα exhibited mainly a random coil structure even though the existence of a nascent bend was detected between residues 30 and 36 by NMR (Figure 6A). Conversely, in the presence of β-TrCP protein, the NMR and molecular modeling calculations performed firmly established that 24P-IκBα adopts a well-defined three-dimensional structure consisting of a central bend, extending from Arg29 to Met37 that is flanked by two turn-structured N- and C-terminal domains (Figure 6B).

Recently, the bound structures of Vpu (*20*) and β-catenin (*21*) have been determined by NMR and molecular modeling. The structure of β-catenin exhibits an N-terminal domain with a tendency to form turns followed by a bend and its C-terminal flexible part. The structure of Vpu also consists of a turn N-terminal region showing a weak helical tendency followed by a bend in the central region and a C-terminal

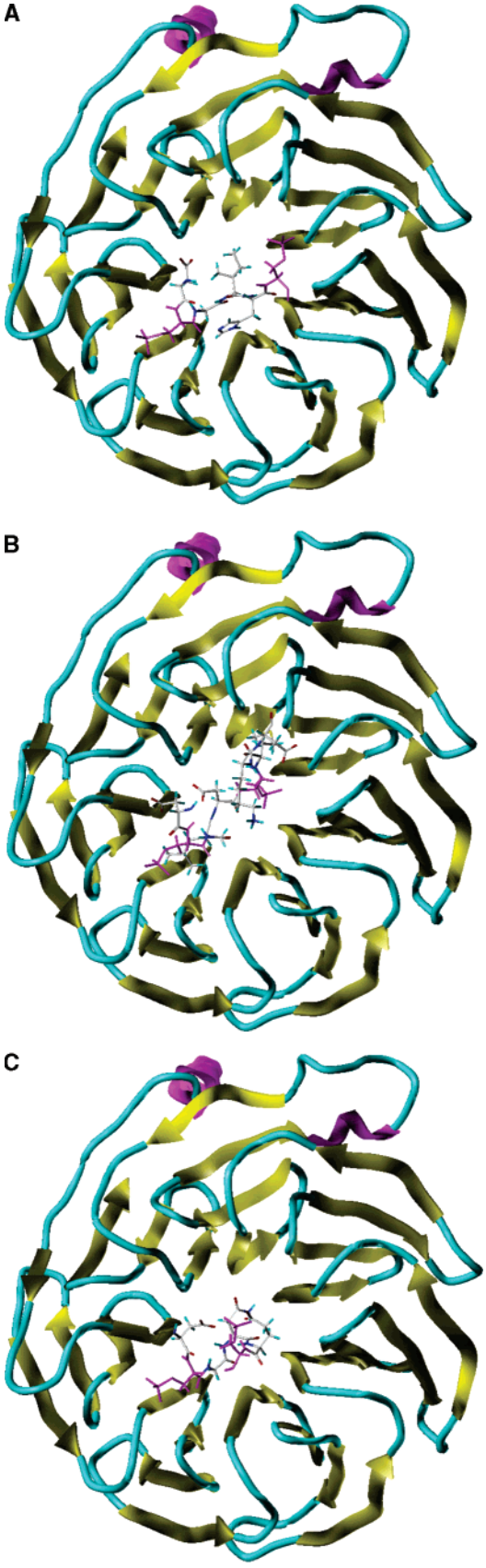

FIGURE 10: Surface representation of the top face of the β-TrCP WD40 domain with the bound D**pS**GXX**pS** motif (A) from the crystal structure of the complex of the human β-TrCP−SkP1 with β-catenin substrate peptide (*45*), (B) from the NMR 24P-IκBα-bound peptide, and (C) from the NMR Vpu-bound peptide (*20*).

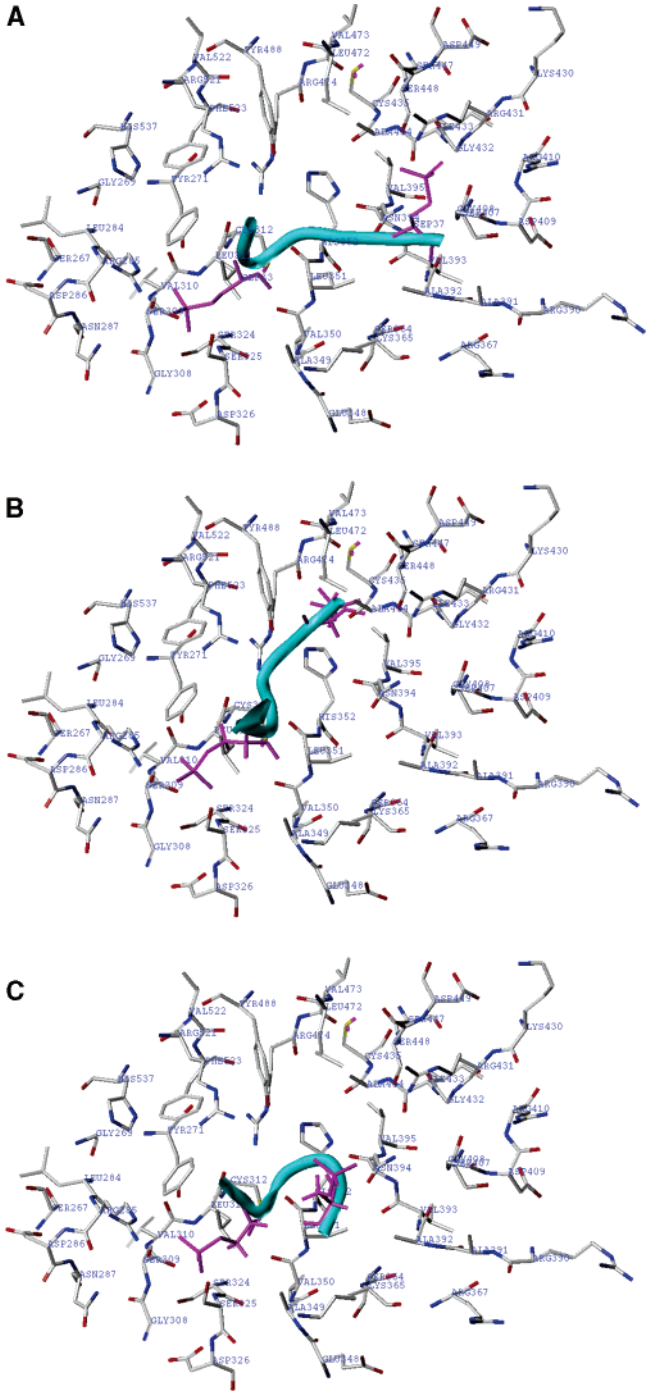

FIGURE 11: A portion of the seven β-propeller structure of the WD40 region of the β-TrCP protein corresponding to the active site is shown with the D**pS**GXX**pS** motif of the substrate peptides. The residues of the protein surface are to 5 Å of the ligand based on the crystal structure of the complex (β-TrCP−SkP1−β-catenin peptide). The first phosphoserine residue of the D**pS**GXX**pS** motif is able to make an electrostatic interaction with the positive Arg285 (WD1) and hydrogen bonds with the hydroxyl groups of Tyr271, Ser309, and Ser325 (WD1). A second broader site formed by a positive charge distribution on the surface Arg367, Arg390, Arg431, and Lys365 (WD3) is able to bind the second phosphoserine. A hydrophobic pocket is composed of the aliphatic portion of the Phe523 and Val516 (WD7) side chains in β-TrCP. (A) The fragment of β-catenin substrate peptide from the crystal structure of the complex bound to the human β-TrCP−SkP1. (B) The fragment of the NMR 24P-IκBα-bound peptide. (C) The fragment of the NMR Vpu-bound peptide.

domain that is unstructured. 24P-IκBα thus shares a common structural organization with β-catenin and Vpu with a central bend flanked by two turn regions. This conserved structural organization suggests that it may play an important role in ligand/receptor interaction. NMR and crystal structures (*20*, *21*, *45*) have shown that the central bend is responsible for the interaction of ligand with its receptors (Figures 10 and 11). The central bend of the D**pS**GXX**pS** motif region is responsible for high-affinity binding, and this suggests that the flexibility of this region of the molecules is an important feature for ligand/receptor interaction (Figure 11). However, an interaction of peptide ligands that involves the turn-structured N-terminal region is required to favorably preposition the peptide. NMR studies have revealed that the N-terminal residues are also implicated in promoting low-affinity binding to the receptor (*20*, *21*). On the basis of our observations, a multiple-site mode of ligand/receptor interaction will be proposed for 24P-IκBα in which the central bend interacts with the WD domain of the receptor and the external loops of the peptide also interact with the receptor.

Epitope Mapping of the 24P-IκBα Peptide. IκB-α, an inhibitory protein that binds to the transcription factor NF-κB, is ubiquitinated and degraded through the proteasome pathway. Two amino acid motifs in IκB-α are known to play important roles in this process: (i) a pair of serines separated by three amino acids (positions 32 and 36), which become phosphorylated prior to proteasome degradation, and (ii) two lysines, which are candidate sites for covalent attachment of ubiquitin, about 10 amino acids upstream of the phosphoserines (*52*). The STD−NMR studies of the IκB-α peptide in the presence of β-TrCP showed the involvement in binding of the NH groups of the negatively charged sequences: the phosphorylated D**pS**^{32}GLD**pS**^{36} motif and fragments involving the residue glutamic acid (E), D**pS**^{36}-MKD**E**^{40} or D**E**^{40}EY**E**^{43}. In addition, the STD enhancements of the NH in the fragment ^{25}LLDDRH^{30} show that hydrophobic Leu26 residue along with charged (Asp27, Asp28, Arg29, and His30) amino acids contact the site. The relative similarity in STD effect (STD intensities between 50% and 100%) shows clearly that these different regions bind strongly to the receptor protein.

The N- (^{25}LLDDRH^{30}) and C-terminal (^{35}D**pS**XXX**E**^{40}) turn regions are clearly important here as is shown by the epitope mapping data (STD NMR). The fact that these residues were close to the known D**pS**GXX**pS** binding fragment enhanced interaction of the IκB-α ligand to β-TrCP protein. Similarities are observed between IκB-α and other proteins known to be degraded by the proteasome pathway (*20*, *21*). The X-ray crystallographic analysis of β-TrCP protein complexed with a fragment β-catenin substrate peptide (*45*) reveals the binding site specific for a phosphopeptide complex bound to a seven-bladed WD40 propeller domain (Figure 10) and that nearly all of the β-TrCP contacts are made by the six residue **pS**GIH**pS** motif. However, the fragment in the complex is too short to highlight a hydrophobic interaction upstream (Figure 10). When we superimposed (Figure 7) this crystal structure on the NMR-determined structures of 24P-IκBα, Vpu (*20*), and β-catenin (*21*) peptides, which have a consensus β-TrCP-binding motif, we found that they fit the binding pocket reasonably well. However we noticed that a different localization affected the second serine.

Similar saturation transfers were observed for 24P-IκBα, Vpu (*20*), and β-catenin (*21*), and one can generally assign two main common parts of the peptides in contact with β-TrCP protein, that is, in the case of 24P-IκBα, the ^{31}D**pS**GLD**pS**^{36} motif region and the upper left region ^{27}-DDRH^{30}. For 24P-IκBα, another group of residues, ^{35}D**pS**MKD**E**^{40}, seem to be important for binding and to be close to the protein surface. This is consistent with the fact that the three regions have shown large STD enhancements. The variations in STD enhancements, especially on both sides of the D**pS**GXX**pS** motif, can be used to differentiate the studied molecules. Also, the discrepancies found between NMR structures of complexes between β-TrCP protein and β-catenin, 24P-IκBα, and Vpu ligands can help in further characterization of these interactions (Figure 10).

The Active Site in the WD Domain of β-TrCP Protein. The C-terminal domain of β-TrCP contains seven WD repeats (Figure 10), known to form interfaces for protein−protein interaction (*53*) and required for optimal binding. Modeling of the F-box protein β-TrCP (*54*) reveals an extensive basic region on the front face of the propeller, which may engage substrate phosphoepitopes. The β-TrCP WD domain has the ability to recognize phosphoserine epitopes in the context of the adjacent glycine residue. The glycine binding pocket is able to accommodate other residues with a same propensity to form β turns. The known factor essential for binding is the phosphate group of the phosphoserine residue (Figure 7), which gives the higher relative saturation transfer (STD signal 100%). In the case of the aspartic acid, arginine, histidine, lysine and glutamic acid, the contact is through the charged groups, whereas in the case of the leucine and methionine, it is a hydrophobic contact. The glycine also participates in binding contact with similar larger STD intensity, 70% (Figure 9). β-TrCP could associate with 24P-IκBα peptide via charge-based interactions. In the DDR^{29}HD**pS**^{32}GLD**pS**^{36}MKDE^{40}E fragment, except for Gly33, Leu34, and Met37, all the chain residues form a charged surface that would provide a plausible binding region in contact with the charged protein β-TrCP surface (Figure 11). The phosphate group of the first phosphoserine can carry out a great number of contacts, in forming direct hydrogen bonds with the side chain hydroxyl groups of Tyr271, Ser309, and Ser325 in the WD domain of β-TrCP protein (Figure 11). The phosphate group forms also direct electrostatic interactions with the guanidium group of Arg285 (Figure 11). This creates a hydrogen bond network in the protein around the phosphate group and can explain the high saturation transfer toward the phosphate group of phosphoserine. On the basis of previous mutational analysis (*18*, *55*, *56*), the arginine residues of β-TrCP protein are essential for function. The lysine or arginine residues of the WD1 fragment would be part of the β-TrCP interaction domain with the acid-rich motif segment negatively charged. To test the specific association between the WD repeat domain of the receptor subunit of the SCF−β-TrCP ubiquitin ligase and a phosphorylated IκBα peptide (P-IκBα), the effect of the lysine mutant residues (WD1, Lys304 and Lys326 replaced with alanine) on binding P-IκBα was examined (*57*). A single WD1 Lys326 mutation has an inhibitory effect on the binding of P-IκBα. Asp31, which is an invariant binding motif residue, is also able to make an extensive contact because its side chain allows a hydrogen bond with Arg521, Arg474,

and Tyr271 in the WD domains. Gly33, also an invariant binding motif residue, is able to pack with the β-TrCP receptor in an environment with little space for a non-glycine residue. The conservation of the Gly33 residue is also justified by the need for compact side chains not to disturb the position of Leu331 and Leu351 of β-TrCP protein. The position of the Leu34 residue in the D**pS**^{32}GLD**pS**^{36} motif (Figure 11), located above the central channel of the seven-bladed WD40 propeller domain and without particular implication of the side chains, can explain the variability of the residues to these positions in the phosphorylation motif. The binding site seems to be enough restricted to select the D**pS**G motif (Arg285, Arg474, Arg521, and some hydrogen bonds) since this part of the motif is relatively hidden and a second broader site formed by a positive charge distribution on the surface (Arg367, Arg390, Arg431 and Lys365) laid out around the second phosphoserine. This positive charge distribution can also highlight the better affinity of P-Vpu compared with the others ligands. The second phosphoserine is less embedded (Figures 7 and 11) and its original orientation in the bound Vpu (Figure 11C) can explain a better interaction of this ligand.

The NMR data described above show that the epitope comprises a surface extending over residues of the bend D**pS**^{32}GLD**pS**^{36} motif of the bound peptide associated with the hydrophobic cluster. Leu25, Leu26, Leu34, and Met37, whose hydrophobic nature is conserved in the peptide fragment, are able to make van der Waals contacts with a hydrophobic pocket that would be composed of the aliphatic portion of the Val516 and Phe523 side chains in β-TrCP (Figure 11).

Inhibitory Effect on β-TrCP Substrates by HIV-1 Vpu. Interaction of the substrates IκB-α, HIV-1 Vpu, and β-catenin with β-TrCP relies on the motif D**pS**GNE**pS**. The WD domain of β-TrCP has positive amino acids, arginine and lysine (Figure 11) that could accept the diphosphorylated segment, D**pS**GXX**pS**, present in the IκB-α, Vpu, and β-catenin proteins. Study of mutations R285E, R474E, R521E, R524E, and K365E made it possible to identify the binding site of IκBα and β-catenin for β-TrCP (*19*). Vpu exerts a generalized inhibitory effect on multiple substrates of β-TrCP and impairs their degradation (*22*, *23*). The sequence similarity between Vpu and IκB-α could result from convergent evolution. Vpu contains a six amino acid diserine motif D**pS**GNE**pS** (positions 51 and 56) that is in a position to interact with β-TrCP protein in the cytoplasm. The diserine motif in Vpu is identical in four positions and has one conservative glutamic acid to aspartic acid change compared with the diserine motif (D**pS**GLD**pS**) in IκB-α. The two serines in this motif are phosphorylated and mutations of these serines in the Vpu block the rapid degradation of CD4 (*58*), as well as mutations in the homologous serines in IκB-α block proteasome-mediated degradation of IκB-α. Nine amino acids upstream of its diserine motif, Vpu contains the sequence DRLIE; in the same relative position, IκB-α contains a closely related repeated sequence ERLLD (E/D change). Both the diserine motif and the DRLIE motif are absent from a truncated version of Vpu that fails to accelerate degradation of CD4 (*13*). Juxtaposed with its diserine motif, Vpu contains the sequence ^{55}E**pS**EX**E**^{59}; in a similar C-terminal position, IκB-α contains a closely related repeated sequence ^{39}D**E**EX**E**^{43} (E/D and E/**pS** change).

Mainly for Vpu, the presence of the negative charged residues in the motif ED**pS**GXE**pS**EGE reinforced the phosphate group interaction to β-TrCP. P-Vpu is the only protein containing as many negative charges in this motif among the others ligands (Figure 11C). The fact that four glutamic acid and one aspartic acid residues were close to the phosphoserine enhanced the negative potential generated by the phosphorylated serine. This negative pole around the phosphate groups of the serine reinforces the Vpu binding to the β-TrCP protein. Indeed, a fragment composed of long negatively charged residues (phosphoserine or glutamic acid) and short aspartic acid residues in close proximity was mainly indicated to interact with β-TrCP protein. Recently, β-TrCP protein was reported to be responsible for the recognition and ubiquitination-dependent degradation of human somatic Wee1, the Cdc2 inhibitory kinase, although Wee1 lacks the consensus D**pS**GXX**pS** binding motif (*59*). Phosphorylation of human somatic Wee1 creates phospho-degrons (signals for degradation) binding to β-TrCP through direct interaction with the basic residues of β-TrCP (*60*). Amino acid residues D**pS**AFQ**E**, E**E**GFG**pS**, and E**E**GFGSS**pS** in Wee1 important for its recognition by β-TrCP may mimic the common binding motif, although in E**E**GXXXX**pS** the residue phosphoserine is located two residues downstream of E**E**GXX**pS**.

In conclusion, by determining conformations of IκB-α, in solution and in interaction with β-TrCP, at the molecular level, we have established that structural differences in the amino acid sequence have an impact to identify key structural parts responsible for competitive inhibition. Because the NF-κB inhibitor protein IκB-α exerts a central role in cellular stress and inflammatory responses, the knowledge of its solution conformation is a first important step toward the design of potent competitors that may have a therapeutic value. Molecules that selectively block recognition of IκB-α by β-TrCP may also constitute an alternative therapeutic target for anti-inflammatory agents.

REFERENCES

1. Karin, M. (1999) How NF-κB is activated: The role of the IκB kinase (IKK) complex, *Oncogene 18*, 6867−6874.
2. Pahl, H. L. (1999) Activators and target genes of Rel/NF-κB transcription factors, *Oncogene 18*, 6853−6866.
3. Barkett, M., and Gilmore, T. D. (1999) Control of apoptosis by Rel/NF-κB transcription factors, *Oncogene 18*, 6910−6924.
4. DeLuca, C., Kwon, H., Lin, R., Wainberg, M., and Hiscott, J. (1999) NF-κB activation and HIV-1 induced apoptosis, *Cytokine Growth Factor Rev. 10*, 235−253.
5. Li, Q., and Verma, I. M. (2002) NF-κB regulation in the immune system, *Nat. Rev. Immunol. 2*, 725−734.
6. Spencer, E., Jiang, J., and Chen, Z. J. (1999) Signal-induced ubiquitination of IκBα by the F-box protein Slimb/β-TrCP, *Genes Dev. 13*, 284−294.
7. Yaron, A., Hatzubai, A., Davis, M., Lavon, I., Amit, S., Manning, A. M., Andersen, J. S., Mann, M., Mercurio, F., and Ben-Neriah, Y. (1998) Identification of the receptor component of the IκBα-ubiquitin ligase, *Nature 396*, 590−594.
8. Hershko, A. (1983) Ubiquitin: Roles in protein modification and breakdown, *Cell 34*, 11−12.
9. Hershko, A., and Ciechanover, A. (1998) The ubiquitin system, *Annu. Rev. Biochem. 67*, 425−479.
10. Weissman, A. M. (2001) Themes and variations on ubiquitylation, *Nat. Rev. Mol. Cell Biol. 2*, 169−178.
11. Margottin, F., Bour, S., Durand, H., Selig, L., Benichou, S., Richard, V., Thomas, D., Strebel, K., and Benarous, R. (1998) A novel human WD protein, h-βTrCP, that interacts with HIV-1 Vpu connects CD4 to the ER degradation pathway through an F-box motif, *Mol. Cell 1*, 565−574.

12. Deshaies, R. J. (1999) SCF and Cullin/Ring H2-based ubiquitin ligases, *Annu. Rev. Cell Dev. Biol. 15*, 435−467.
13. Fujita, K., Omura, S., and Silver, J. (1997) Rapid degradation of CD4 in cells expressing human immunodeficiency virus type 1 Env and Vpu is blocked by proteasome inhibitors, *J. Gen. Virol. 78*, 619−625.
14. Schubert, U., Anton, L. C., Cox, J. H., Bour, S., Bennink, J. R., Orlowski, M., Strebel, K., and Yewdell, J. W. (1998) CD4 glycoprotein degradation induced by human immunodeficiency virus type-1 Vpu protein requires the function of proteasomes and the ubiquitin-conjugating pathway, *J. Virol. 72*, 2280−2288.
15. Latres, E., Chiaur, D. S., and Pagano, M. (1999) The human F box protein β-Trcp associates with the Cul1/Skp1 complex and regulates the stability of β-catenin, *Oncogene 18*, 849−854.
16. Margottin, F., Benichou, S., Durand, H., Richard, V., Liu, L. X., Gomas, E., and Benarous, R. (1996) Interaction between the cytoplasmic domains of HIV-1 Vpu and CD4: Role of Vpu residues involved in CD4 interaction and in vitro CD4 degradation, *Virology 223*, 381−386.
17. Brown, K., Gerstberger, S., Carlson, L., Franzoso, G., and Siebenlist, U. (1995) Control of I κ B-α proteolysis by site-specific, signal-induced phosphorylation, *Science 267*, 1485−1488.
18. Nash, P., Tang, X., Orlicky, S., Chen, Q., Gertler, F. B., Mendenhall, M. D., Sicheri, F., Pawson, T., and Tyers, M. (2001) Multisite phosphorylation of a CDK inhibitor sets a threshold for the onset of DNA replication, *Nature 414*, 514−521.
19. Zhang, J., Zheng, N., and Zhou, P. (2003) Exploring the functional complexity of cellular proteins by protein knockout, *Proc. Natl. Acad. Sci. U.S.A. 100*, 14127−14132.
20. Coadou, G., Gharbi-Benarous, J., Megy, S., Bertho, G., Evrard-Todeschi, N., Segeral, E., Benarous, R., and Girault, J. P. (2003) NMR studies of the phosphorylation motif of the HIV-1 protein Vpu bound to the F-box protein β-TrCP, *Biochemistry* 14741−14751.
21. Megy, S., Bertho, G., Gharbi-Benarous, J., Baleux, F., Benarous, R., and Girault, J. P. (2005) STD and TRNOESY NMR studies on the conformation of the oncogenic protein β-catenin containing the phosphorylated motif DpSGXXpS bound to the β-TrCP protein, *J. Biol. Chem. 280*, 29107−29116.
22. Bour, S., Perrin, C., Akari, H., and Strebel, K. (2001) The human immunodeficiency virus type 1 Vpu protein inhibits NF-κ B activation by interfering with β TrCP-mediated degradation of Iκ B, *J. Biol. Chem. 276*, 15920−15928.
23. Besnard-Guerin, C., Belaidouni, N., Lassot, I., Segeral, E., Jobart, A., Marchal, C., and Benarous, R. (2004) HIV-1 Vpu sequesters β-transducin repeat-containing protein (βTrCP) in the cytoplasm and provokes the accumulation of β-catenin and other SCFβTrCP substrates, *J. Biol. Chem. 279*, 788−795.
24. Clore, G. M., and Gronenborn, A. M. (1982) Theory and applications of the transferred nuclear Overhauser effect to the study of the conformations of small ligands bounds to proteins, *J. Magn. Reson. 48*, 402−417.
25. Clore, G. M., and Gronenborn, A. M. (1983) Theory of the time dependent transferred nuclear Overhauser effect: Applications to structural analysis of ligand-protein complexes in solution, *J. Magn. Reson. 53*, 423−442.
26. Mayer, M., and Meyer, B. (1999) Characterization of ligand binding by saturation transfer difference NMR spectroscopy, *Angew. Chem., Int. Ed. 38*, 1784−1788.
27. Mayer, M., and Meyer, B. (2001) Group epitope mapping by saturation transfer difference NMR to identify segments of a ligand in direct contact with a protein receptor, *J. Am. Chem. Soc. 123*, 6108−6117.
28. Braunschweiler, L., and Ernst, R. R. (1983) Coherence transfer by isotropic mixing: application to proton correlation spectroscopy, *J. Magn. Reson. B53*, 521−528.
29. Kumar, A., Ernst, R. R., and Wüthrich, K. (1980) A two-dimensional nuclear Overhauser enhancement (2D NOE) experiment for the elucidation of complete proton-proton cross-relaxation networks in biological macromolecules, *Biochem. Biophys. Res. Commun. 95*, 1−6.
30. Bodenhausen, G., and Ruben, D. J. (1980) Natural abundance N-15 NMR by enhanced heteronuclear spectroscopy, *Chem. Phys. Lett. 69*, 185−189.
31. Bax, A., and Summers, M. F. (1986) 1H and 13C assignments from sensitivity-enhanced detection of heteronuclear multi-bond connectivity by 2D multiple quantum NMR, *J. Am. Chem. Soc. 108*, 2093−2094.
32. Bax, A., and Davis, D. G. (1985) MLEV-17-based two-dimensional homonuclear magnetization transfer spectroscopy, *J. Magn. Reson. 65*, 355−360.
33. Marion, D., Ikura, M., Tschudin, R., and Bax, A. (1989) Rapid recording of 2D NMR-spectra without phase cycling - application to the study of hydrogen-exchange in proteins, *J. Magn. Reson. 85*, 393−399.
34. Piotto, M., Saudek, V., and Sklenar, V. (1992) Gradient-tailored exitation for single-quantum NMR spectroscopy of aqueous solutions, *J. Biomol. NMR 2*, 661−665.
35. Wüthrich, K. (1986) *NMR of Proteins and Nucleic Acids*, John Wiley & Sons, New York.
36. Meyer, B., and Peters, T. (2003) NMR spectroscopy techniques for screening and identifying ligand binding to protein receptors, *Angew. Chem., Int. Ed. 42*, 864−890.
37. Nilges, M., and O'Donoghue, S. (1998) Ambigous NOES and automated NOES assignment, *Prog. NMR Spectrosc. 32*, 107−139.
38. Linge, J., and Nilges, M. (1999) Influence of nonbonded parameters on the quality of NMR structures: a new force field for NMR determination, *J. Biomol. NMR 13*, 51−59.
39. Linge, J. P., O'Donoghue, S. I., and Nilges, M. (2001) Automated assignment of ambiguous nuclear overhauser effects with ARIA, *Methods Enzymol. 339*, 71−90.
40. Nilges, M. (1995) Calculation of protein structures with ambiguous distance restraints. Automated assignment of ambiguous NOE crosspeaks and disulphide connectivities, *J. Mol. Biol. 245*, 645−660.
41. Nilges, M., Macias, M. J., O'Donoghue, S. I., and Oschkinat, H. (1997) Automated NOESY interpretation with ambiguous distance restraints: the refined NMR solution structure of the pleckstrin homology domain from β-spectrin, *J. Mol. Biol. 269*, 408−422.
42. Vranken, W., Tolkatchev, D., Xu, P., Tanha, J., Chen, Z., Narang, S., and Ni, F. (2002) Solution structure of a llama single-domain antibody with hydrophobic residues typical of the VH/VL interface, *Biochemistry 41*, 8570−8579.
43. Laskowski, R. A., Rullmann, J. A. C., MacArthur, M. W., Kaptein, R., and Thornton, J. M. (1996) AQUA and PROCHECK-NMR: Programs for checking the quality of protein structures solved by NMR, *J. Biomol. NMR 8*, 477−486.
44. Koradi, R., Billeter, M., and Wüthrich, K. (1996) MOLMOL: A program for display and analysis of macromolecular structures, *J. Mol. Graphics 14*, 51−55.
45. Wu, G., Xu, G., Schulman, B. A., Jeffrey, P. D., Harper, J. W., and Pavletich, N. P. (2003) Structure of a β-TrCP1-Skp1-β-catenin complex: Destruction motif binding and lysine specificity of the SCF(β-TrCP1) ubiquitin ligase, *Mol. Cell 11*, 1445−1456.
46. Wishart, D. S., Bigam, C. G., Yao, J., Abildgaard, F., Dyson, H. J., Oldfield, E., Markley, J. L., and Sykes, B. D. (1995) 1H, 13C, and 15N chemical shift referencing in biomolecular NMR, *J. Biomol. NMR 6*, 135−140.
47. Ni, F. (1994) Recent developments in transferred NOE methods, *Prog. Nucl. Magn. Reson. Spectrosc. 26*, 517−606.
48. Verdier, L., Gharbi-Benarous, J., Bertho, G., Evrard-Todeschi, N., Mauvais, P., and Girault, J.-P. (2000) Dissociation-equilibrium constant and bound conformation for weak antibiotic binding interaction with different bacterial ribosomes, *J. Chem. Soc., Perkin. Trans. 2*, 2363−2371.
49. Kumar, A., Wagner, G., Ernst, R. R., and Wüthrich, K. (1981) Buildup rates of the NOE measured by 2D proton magnetic resonance spectroscopy: Implication for studies of protein conformation, *J. Am. Chem. Soc. 103*, 3654−3658.
50. Peng, J. W., Moore, J., and Abdul-Manan, N. (2004) NMR experiments for lead generation in drug discovery, *Prog. Nucl. Magn. Reson. Spectrosc. 44*, 225−256.
51. Moller, H., Serttas, N., Paulsen, H., Burchell, J. M., Taylor-Papadimitriou, J., and Meyer, B. (2002) NMR-based determination of the binding epitope and conformational analysis of MUC-1 glycopeptides and peptides bound to the breast cancer-selective monoclonal antibody SM3, *Eur. J. Biochem. 269*, 1444−1455.
52. Scherer, D. C., Brockman, J. A., Chen, Z., Maniatis, T., and Ballard, D. W. (1995) Signal-induced degradation of I κ B α requires site-specific ubiquitination, *Proc. Natl. Acad. Sci. U.S.A. 92*, 11259−11263.
53. Neer, E. J., Schmidt, C. J., Nambudripad, R., and Smith, T. F. (1994) The ancient regulatory-protein family of WD-repeat proteins, *Nature 371*, 297−300.
54. Yaffe, M. B., and Elia, A. E. (2001) Phosphoserine/threonine-binding domains, *Curr. Opin. Cell Biol. 13*, 131−138.

55. Spruck, C. H., Strohmaier, H., Sangfelt, O., Muller, H. M., Hubaleck, M., Muller-Hozner, E., Marth, C., Widschwendter, M., and Reed, S. I. (2002) hCDC4 gene mutations in endometrial cancer, *Cancer Res. 62*, 4535−4539.
56. Strohmaier, H., Spruck, C. H., Kaiser, P., Won, K. A., Sangfelt, O., and Reed, S. I. (2001) Human F box protein hCdc4 targets cyclin E for proteolysis and is mutated in a breast cancer cell line, *Nature 413*, 316−322.
57. Davis, M., Hatzubai, A., Andersen, J. S., Ben-Shushan, E., Zvi Fisher, G., Yaron, A., Bauskin, A., Mercurio, F., Mann, M., and Ben-Neriah, Y. (2002) Pseudosubstrate regulation of the SCF$^{\beta-\mathrm{TrCP}}$ ubiquitin ligase by hnRNP-U, *Genes Dev. 16*, 439−451.
58. Schubert, U., and Strebel, K. (1994) Differential activities of the human immunodeficiency virus type I-encoded Vpu protein are regulated by phosphorylation and occur in different cellular compartiments, *J. Virol. 68*, 2260−2271.
59. Watanabe, N., Arai, H., Nishihara, Y., Taniguchi, M., Hunter, T., and Osada, H. (2004) M-phase kinases induce phospho-dependent ubiquitination of somatic Wee1 by SCFβ-TrCP, *Proc. Natl. Acad. Sci. U.S.A. 101*, 4419−4424.
60. Watanabe, N., Arai, H., Iwasaki, J., Shiina, M., Ogata, K., Hunter, T., and Osada, H. (2005) Cyclin-dependent kinase (CDK) phosphorylation destabilizes somatic Wee1 via multiple pathways, *Proc. Natl. Acad. Sci. U.S.A. 102*, 11663−11668.
61. Kroll, M., Margottin, F., Kohl, A., Renard, P., Durand, H., Concordet, J.-P., Bachelerie, F., Arenzana-Seisdedos, F., and Benarous, R. (1999) Inducible degradation of IκBα by the proteasome requires interaction with the F-box protein h-βTrCP, *J. Biol. Chem. 274*, 7941−7945.

BI061401F